
FEDSYNTHCT-BRAIN: A FEDERATED LEARNING FRAMEWORK FOR MULTI-INSTITUTIONAL BRAIN MRI-TO-CT SYNTHESIS

Ciro Benito Raggio*

Institute of Biomedical Engineering
Karlsruhe Institute of Technology
Fritz-Haber-Weg 1, Karlsruhe 76131
Baden-Württemberg, Germany
ciro.raggio@kit.edu

Mathias Krohmer Zabaleta

Institute of Biomedical Engineering
Karlsruhe Institute of Technology
Fritz-Haber-Weg 1, Karlsruhe 76131
Baden-Württemberg, Germany

Nils Skupien

Institute of Biomedical Engineering
Karlsruhe Institute of Technology
Fritz-Haber-Weg 1, Karlsruhe 76131
Baden-Württemberg, Germany

Oliver Blanck

Department of Radiation Oncology
University Medical Center Schleswig-Holstein
Feldstrasse 21, Kiel 24105
Schleswig-Holstein, Germany

Francesco Cicone

Department of Experimental and Clinical Medicine
Magna Graecia University
Viale Europa, Catanzaro 88100
Italy

Giuseppe Lucio Cascini

Department of Experimental and Clinical Medicine
Magna Graecia University
Viale Europa, Catanzaro 88100
Italy

Paolo Zaffino

Department of Experimental and Clinical Medicine
Magna Graecia University
Viale Europa, Catanzaro 88100
Italy

Lucia Migliorelli

Department of Information Engineering
Università Politecnica delle Marche
Via Breccie Bianche 12, Ancona 60131
Italy

Maria Francesca Spadea

Institute of Biomedical Engineering
Karlsruhe Institute of Technology
Fritz-Haber-Weg 1, Karlsruhe 76131
Baden-Württemberg, Germany

December 10, 2024

ABSTRACT

The generation of Synthetic Computed Tomography (sCT) images has become a pivotal methodology in modern clinical practice, particularly in the context of Radiotherapy (RT) treatment planning. The use of sCT enables the calculation of doses, pushing towards Magnetic Resonance Imaging (MRI) guided radiotherapy treatments. Moreover, with the introduction of MRI-Positron Emission Tomography (PET) hybrid scanners, the derivation of sCT from MRI can improve the attenuation correction of PET images. Deep learning methods for MRI-to-sCT have shown promising results, but their reliance on single-centre training dataset limits generalisation capabilities to diverse clinical settings. Moreover, creating centralised multicentre datasets may pose privacy concerns. To solve

*Corresponding author

the issues, this study introduces FedSynthCT-Brain, a framework based on the Federated Learning (FL) paradigm for MRI-to-sCT in brain imaging. We reproduced a federation across four European and American centres using a U-Net-based model. The approach was implemented using data from centres belonging to the federation and it was tested on an unseen dataset from a centre outside the federation. In the case of the unseen centre, the federated model achieved a median Mean Absolute Error (MAE) of 102.0 HU across 23 patients, with an interquartile range of 96.7 – 110.5 HU. The median (interquartile range) for the Structural Similarity Index (SSIM) and the Peak Signal to Noise Ratio (PSNR) were 0.89 (0.86 – 0.89) and 26.58 (25.52 – 27.42), respectively. The analysis of the results showed acceptable performances of the federated approach, thus highlighting the potential of FL to enhance MRI-to-sCT to improve generalisability and advancing safe and equitable clinical applications while fostering collaboration and preserving data privacy.

Keywords Federated Learning · Medical Image Synthesis · Synthetic Computed Tomography · Deep Learning · Image-To-Image Translation · Data Sharing · Data Privacy

1 Introduction

Intermodality medical Image-To-Image (I2I) translation refers to the process of mapping images from one modality (e.g., Magnetic Resonance Imaging - MRI, Computed Tomography - CT, Positron Emission Tomography - PET) to another, while preserving essential structural and anatomical information. Deep Learning (DL) based techniques have been shown to outperform traditional methods based on image registration and/or voxel-wise analysis [10] and they have gained attention in several clinical fields, the most important being the derivation of Synthetic CT (sCT) from MRI or Cone Beam CT (CBCT), to facilitate radiotherapy planning/adaptation or to improve attenuation correction in PET/MRI acquisition [49, 52].

Despite the advancements in DL-based I2I, several critical limitations remain. Indeed, current DL approaches are trained on datasets that represent specific patient populations, which hampers their generalizability across different clinical settings [37, 14, 41, 4]. For instance, the training datasets often exclude patients with implants or atypical anatomy, resulting in synthetic CTs that are less reliable for these unique cases [15]. Additionally, single-site models tend to underperform when applied to images from different medical centres, as they are sensitive to domain shifts in imaging protocols, scanner types, and patient demographics [9].

To improve generalizability in MRI-to-sCT and foster innovation in the field, initiatives like the SynthRAD2023 [21] challenge have been proposed by the scientific community. These efforts allow DL models — such as the MSEP framework, the challenge winner [20, 8] — to be trained on multi-centre datasets, providing access to more diverse patient data. While directly pooling medical images from multiple sites could intuitively address the issue of small sample sizes, this approach faces significant barriers due to stringent privacy protection policies such as the Health Insurance Portability and Accountability Act (HIPAA)² in the United States and the General Data Protection Regulation (GDPR)³ in Europe. These regulations impose limitations on the exchange of personal health data, posing practical challenges to sharing and centralising medical images across sites [23, 16].

The presence of bias from limited diversity in images from a single institution, along with concerns about data centralisation, underscores the need for a collaborative approach that enables access to substantial amounts of data without centralising it [1].

Federated Learning (FL) can overcome data-sharing barriers by allowing multiple institutions to train a DL model collaboratively without sharing their own data on a central server. This approach both facilitates secure data collaboration and also leverages distributed computing resources to strengthen model generalizability across diverse, unseen datasets [17].

Given these premises, the aim of the proposed study was to establish a FL framework for MRI-to-sCT, which we call FedSynthCT, and to prove its validity in the context of brain imaging (henceforth we will refer to our approach as FedSynthCT-Brain).

A benchmark analysis was conducted across multiple architectures and different aggregation strategies in order to assess the trade-offs between efficiency and effectiveness for realistic clinical applications.

To the best of the authors' knowledge, this is among the first application in literature to employ a FL paradigm in MRI-to-sCT. The main contributions of the work are:

²<https://www.hhs.gov/hipaa/index.html>

³<https://gdpr-info.eu/>

- We propose a cross-silo horizontal FL approach for MRI-to-sCT in brain imaging, where data of the same type (horizontal FL) from various centers, or “silos” is collaboratively used to train a DL model.
- We validate the proposed approach on real multi-centre data, simulating an authentic scenario where each centre handles heterogeneous data, due to different scanners and acquisition modalities.
- We evaluate the proposed FedSynthCT-Brain on an independent dataset outside the federation to assess its generalization capability on data from external centres, demonstrating its effectiveness even in the presence of significant data heterogeneity.

The structure of this paper is as follows: Section 2 reviews existing research on computer-aided MRI-to-sCT and the use of FL for the task of medical-image analysis. Section 3 outlines the dataset and the proposed FedSynthCT-Brain approach. The experimental setup is detailed in Section 4. Section 5 presents the results, with further discussion in Section 6. Finally, Section 7 summarizes the main findings and the impact of the proposed research while proposing future directions.

2 Related work

2.1 Centralised MRI-to-sCT

Over the past years, numerous DL methods have been implemented for MRI-to-sCT. The proposed model architectures and methodologies have become increasingly complex in order to achieve accurate results. Among the most widely used models are: U-Nets, Generative Adversarial Networks (GANs), Transformers, and Diffusion-based architectures [10].

Several works employed three different 2-dimensional (2D) fully Convolutional Neural Networks (CNN), one for each anatomical plane (axial, coronal, and sagittal), to retain structural information in sCTs while simultaneously reducing computational costs, especially when using U-Nets [10, 28, 50, 19]. These 2D methods, by processing slices independently or in parallel, inherently simplify training in distributed environments, such as FL, where data sharing is constrained by computational heterogeneity [3].

On the other side, 3D-DL approaches have demonstrated improved spatial continuity and consistency in terms of Hounsfield Unit (HU) across slices compared to their 2D akin [10]. However, the primary limitation of 3D models lies in their higher computational demand, which requires splitting volumetric data into smaller 3D patches for processing [26, 25]. This patch-based processing may lead to the loss of global context and structural coherence, especially when patches are analysed in isolation. Moreover, the scalability of 3D approaches in FL settings is further constrained due to the increased communication overhead and memory requirements associated with volumetric data. These factors make 3D-DL approaches less suitable for FL real-world scenarios where limited computational resources requirements must be accounted for [3].

2.2 Federated learning in medical imaging

The growing number of studies applying FL in healthcare, particularly in medical imaging [16, 47, 31, 27, 6], reflects its increasing importance. By keeping sensitive information, such as patient data, within local environments (e.g., clinical centres), FL addresses the crucial need for confidentiality in medical applications, enabling collaborative large-scale model development without data sharing.

The partitioning of data is of pivotal importance in this context, particularly in the domain of medical imaging, where datasets are frequently scarce, heterogeneous, and non-Independent and Identically Distributed (non-IID). Data imbalance has the potential to significantly impact model generalisation and performance across institutions, as medical images from disparate sources are susceptible to bias due to differences in equipment, protocols, and labelling processes. FL addresses these challenges by aggregating models from various institutions, thereby mitigating bias and improving generalisability [46].

Several studies investigated the use of FL on medical images, especially for classification and segmentation tasks.

In the field of classification, FL has been applied X-ray and CT images for the diagnosis of COVID-19 [12, 60]. Furthermore, numerous studies have focused also on the classification of skin diseases and lesions [58, 18], prostate classification [59, 58], as well as in the ophthalmology field for the diabetic retinopathy classification [39].

More recently, FL approaches were proposed for segmentation tasks, such as for brain tumour [53, 2], prostate [61], optic cup and disc segmentation [43, 55]. This led to the development of frameworks that integrate the aforementioned works and are capable of performing segmentations of multiple anatomical structures or different image modalities using FL and foundational models, such as the FedFMS [38].

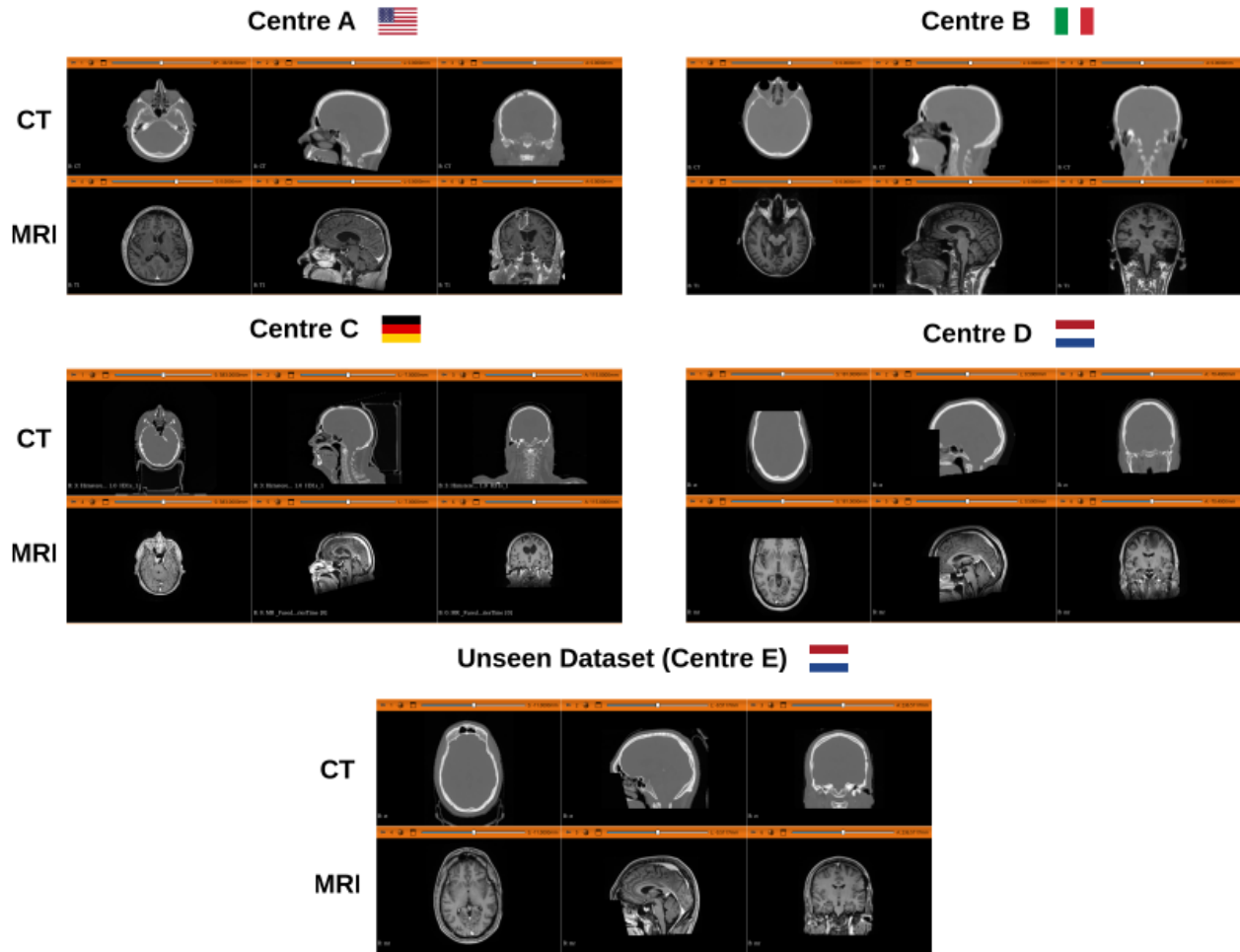


Figure 1: Visual comparison of image appearance across datasets from multiple Centres. The FOV of the images from Centre A was limited to the level of the mouth and included partial cut-off of the ears. Images from centre B were acquired using a PET-MRI hybrid scanner. Furthermore the higher CT slice thickness introduced partial volume artefacts in the skull bone reconstruction. Images coming from centre C exhibited higher spatial resolution in the cranial caudal direction, but presented other problems, including partial cropping at the top of the skull and metal artefacts. Centres D and E—derived from SynthRAD2023 challenge—shared similar imaging regions with less bias fields compared to Centre C.

Recent advancements in medical image synthesis have introduced innovative methods, such as FedMed-GAN, which specifically addresses the challenge of synthesizing cross-modality brain MRI images in an FL setting [56]. It employs FedAvg as the aggregation strategy, enabling the combination of locally trained models from multiple institutions.

Inspired by the FL paradigm, this study explores the potential of FL for MRI-to-CT synthesis, tackling a challenge that remains unaddressed in existing research.

3 Methods

3.1 Datasets and preprocessing

For each centre (named A, B, C, D and E) a dataset containing paired, co-registered MRI T1-weighted and CT images was available. Image acquisition was performed in accordance with the ethical standards of the 1964 Declaration of Helsinki and later amendments. Written informed consent to use data for research purposes was obtained from all patients. The image acquisition protocol and scanners differed among the various centres, as it is reported in Table 1. This led to image variability among the federated dataset and the most relevant difference can be appreciated in Figure 1.

Data origin	Patient #	Image modality - Voxel size [mm ³]	Size		
			Axial	Sagittal	Coronal
Centre A (USA)	15	MR - $1 \times 1 \times 1$ CT - $0.49 - 0.67 \times 0.49 - 0.67 \times 2.5$	256	176	256
Centre B (IT)	14	MR - $1 \times 1 \times 1$ CT - $0.98 \times 0.98 \times 3.27$	256	176	248
Centre C (DE)	21	MR - $0.78 \times 0.78 \times 1$ CT - $0.78 \times 0.78 \times 1$	226 - 357	512	512
Centre D (NL, SynthRAD Centre C [21])	29	MR - $0.98 - 1.12 \times 0.98 - 1.12 \times 0.98 - 1.12$ CT - $0.69 - 0.78 \times 0.69 - 0.79 \times 1 - 3$	167 - 213	216 - 262	250 - 277
Centre E (NL, SynthRAD Centre B [21])	23	MR - $0.98 \times 0.98 \times 0.98$ CT - $0.59 - 1.27 \times 0.59 - 1.27 \times 1 - 2$	167 - 262	200 - 225	225 - 248
Data origin	MRI scanners / Field strength [T]	CT scanners / kVp			
Centre A (USA)	MAGNETOM Trio / 3	LightSpeed QX/i / 140			
Centre B (IT)	Biograph mMR / 3	Discovery ST / 120			
Centre C (DE)	Vantage Titan / 1.5	Brilliance Sensation Open / 120			
Centre D (NL, SynthRAD Centre C [21])	MAGNETOM, Avanto_fit, Skyra, Vida_fit, Prisma_fit / 1.5-3	Brilliance Big Bore / 120			
Centre E (NL, SynthRAD Centre B [21])	MAGNETOM Aera, Avanto_fit / 1.5-3	SOMATOM Definition AS / 120			

Table 1: Summary of the most relevant characteristics of the image datasets used in the federated learning (FL) framework. Data from Centre A, B, C, and D were used to train the federated model; thus Centre A, B, C, D acted as clients. The data from the Centre E (SynthRAD Centre B) served as an independent dataset for testing the generalisability of the federated model on unseen data. For each dataset we list the number of patients, image sizes, magnetic resonance imaging (MRI) and computed tomography (CT) scanners used, and voxel spacing in millimeters.

The field of view (FOV) of images from Centre A started at the mouth region with a straight cut off and spans towards the top of the skull. A fraction of the ears was also cut off.

MRIs from Centre B were acquired using a PET-MRI hybrid scanner. Differently from the other centres, this acquisitions were not performed for radiotherapy planning purposes. Thus, the tube energy in the CT was 120kV and the slice thickness was 3.75 mm which introduced partial volume artifacts in the upper part of the skull bone. In light of the substantial difference in the acquisition protocol and scanners, Centre B dataset was used to increase the image variability within the federation (i.e. to introduce noise) to test the robustness of the federated model and simulate a real context.

Images belonging to Centre C presented higher spatial resolution in the cranial caudal direction compared to the other datasets. However, the Centre C’s dataset presented a number of additional challenges, including: the absence of the top of the skull in some patients, the presence of the scanner bed and pillow for each CT, metal artefacts, and high bias field artifact.

The Centre D’s and Centre E’s datasets derived exclusively from two different institutions of the SynthRAD2023 multi-centre dataset (SynthRAD Centre C and SynthRAD Centre B respectively), which was created for the SynthRAD challenge within different MRI-to-sCT algorithms [21]. Before publication, the datasets were cropped to remove the facial region. TheFOV covered by both imaging modalities was similar, except for a cut-off at the lower end with a slight angle in addition to a straight horizontal line. In general, Center D and E presented less bias field artifact when compared to Center C. However, between Centre D and E, it was more pronounced in the Centre E dataset. Furthermore, both Centre MRIs were obtained using gadolinium-based contrast agents, thus introducing further heterogeneity within the federation.

To address the image variability, a pre-processing strategy was implemented at each client site with the aim of harmonising data within the federation, without the exchange of data. Following [54], N4 Bias Field Correction was applied to the MRI data to correct intensity inhomogeneity, which can result from factors such as magnetic field variations or patient positioning. Additionally, Min-Max Normalization was applied within each client to reduce variability in pixel intensity values.

Due to the differences in acquisition protocols, the datasets included images of varying dimensions (See Table 1). To standardize input for the federated model, all image volumes were cropped, resized, and padded to a uniform size of $256 \times 256 \times 256$ voxels (See Section 4). This process enabled each client to preprocess its data independently while maintaining a consistent input format across the federation, thereby allowing seamless aggregation of the DL model updated from each client.

The elements outside the patient body (couch, immobilisation system, pillow) were masked out on the CT volume using 3D Slicer image computing platform [11] (Figure 2). The obtained mask was applied also to the corresponding MRI to remove background noise. Voxels outside the mask were set to -1000 and 0 for CT and MRI respectively.

3.2 Federation setup

As shown in Figure 3, we created a FL environment to simulate a realistic collaboration involving 4 distinct clients, each representing a different clinical centre as outlined. In this setup, each client trained a local DL model on its own data, while a central server coordinated the creation of a federated model. This federated model was built by aggregating key parameters (e.g., weights, biases, and batch normalization parameters) from each local model after every local training round, effectively combining weights from all clients without sharing raw data. The aggregated model parameters were then redistributed to each client, enhancing their local models with information learned across all sites.

To evaluate generalisation, the federated model was tested on an independent dataset from a fifth centre, which none of the clients had access to during training.

3.3 Deep learning model

Following preliminary experiments (see Section 4.4.1), the DL architecture employed in the proposed FL framework was the U-Net model proposed by Li et al. [34]. The network is a residual learning based U-Net, designed to predict 256×256 sCT 2D slices from 256×256 MR inputs. The architecture comprises 34 convolutional layers, starting with a 7×7 convolutional layer for initial feature extraction, followed by multiple 3×3 convolutional layers.

A key feature of the architecture dealt with the inclusion of residual blocks, which consisted of two 3×3 convolutional layers, each followed by batch normalization and rectified linear unit (ReLU) activation, and a short skip connection that added the input of the block to its output to improve gradient propagation and enable efficient training. In the encoder path, max-pooling operations were used for downsampling the dimensions of the feature maps, doubling the

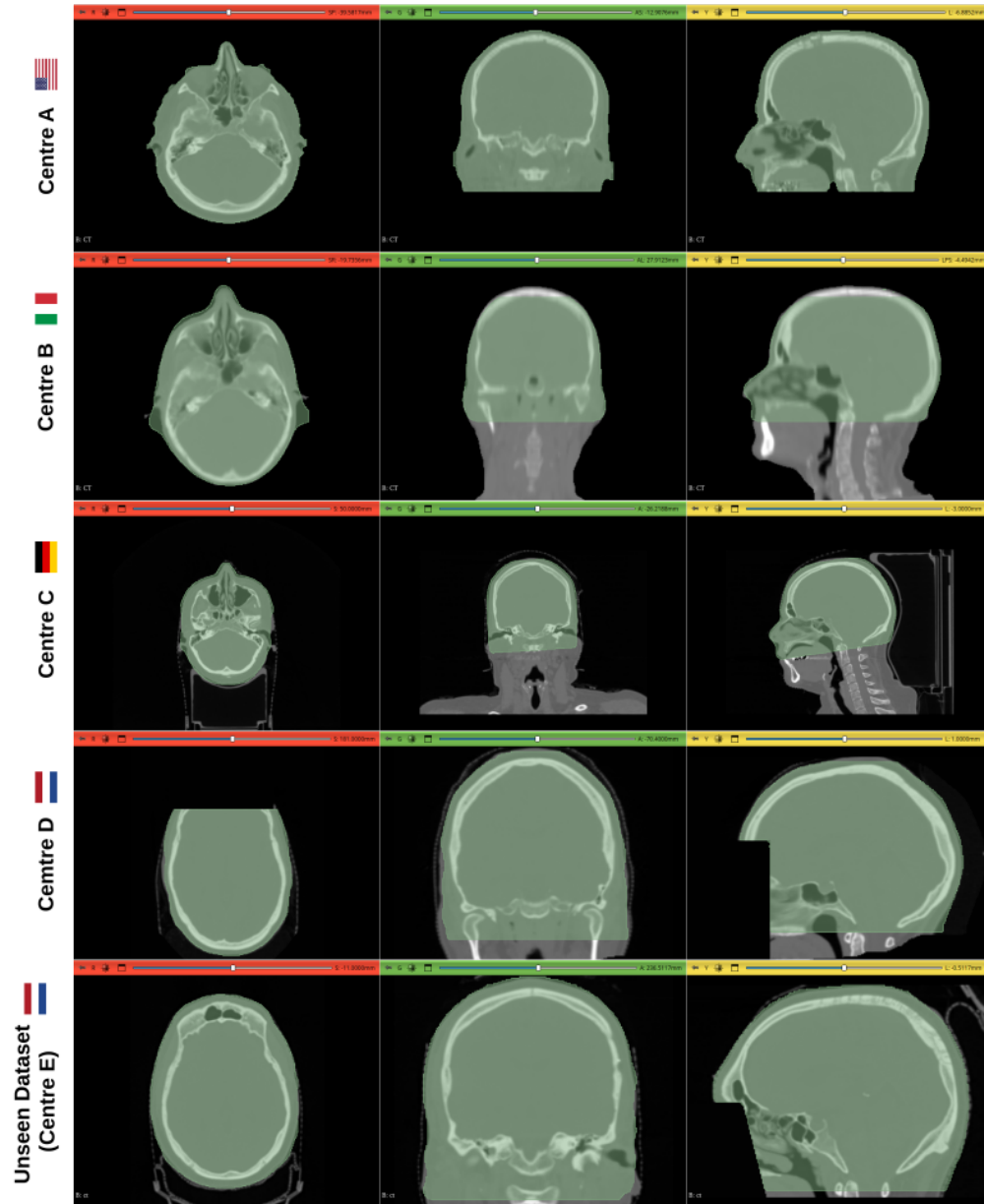


Figure 2: The figure illustrates the background masking for each institution. By eliminating potential misleading features for the model, the masking approach limits the prediction of the model to areas of interest and facilitates the harmonisation of the model’s knowledge within the federation. The masking process was conducted within the individual Centre. The parts of interest were established beforehand, as would be done in a real-world context.

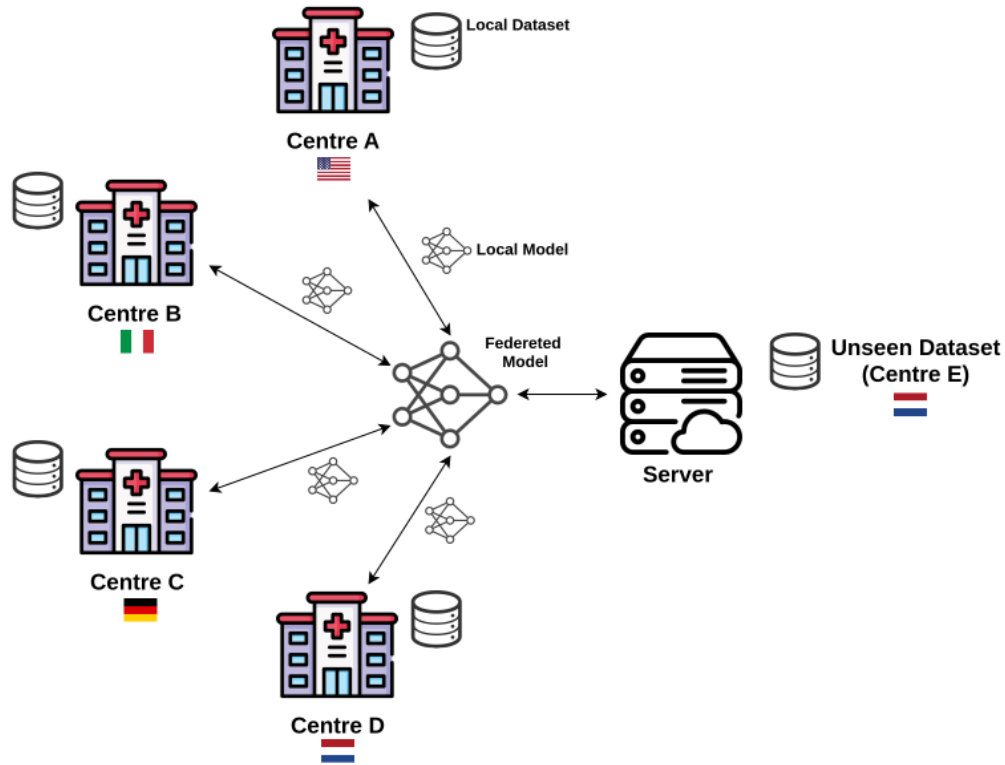


Figure 3: Federated setup. Each centre (also called client) has its own local data and trains a model on the local dataset. The weights of the local model are exchanged with the server, which, after the aggregation process, returns a federated model to the clients. The server also hosts a dataset that is not used during training, but acts as a benchmark to determine the generalisation ability of the model.

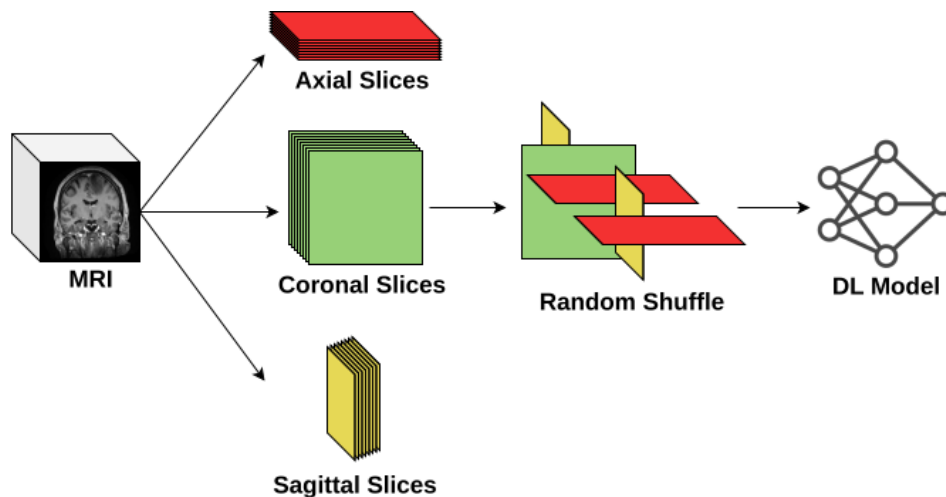


Figure 4: Proposed training methodology. The pre-processed and augmented 3D (MRI) volume is subdivided into 2D slices, extracted along the three anatomical planes (sagittal, axial, coronal). These slices are then subjected to a random shuffling process, ensuring that the model is agnostic with respect to both the anatomical plane and the imaging sequence. The shuffled batch of images is then provided as input to the model.

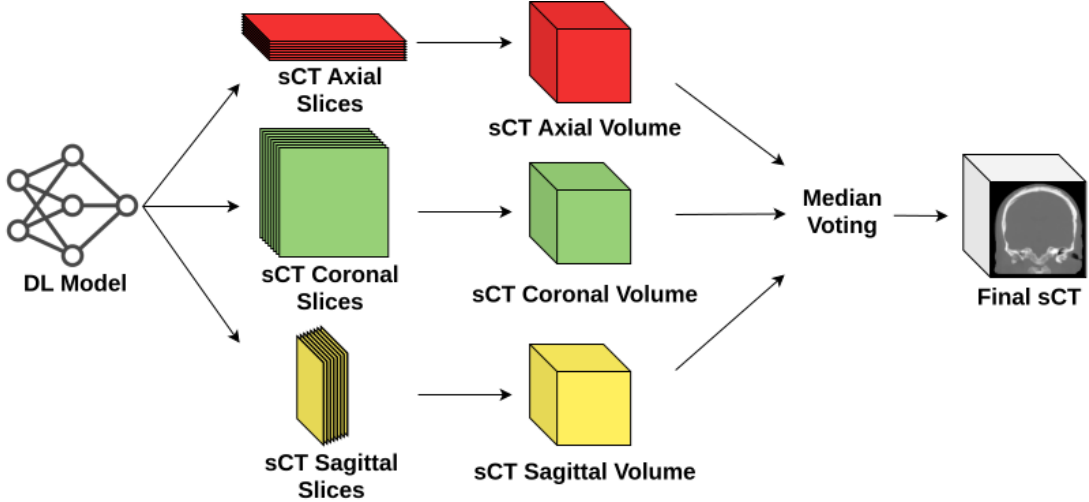


Figure 5: Reconstruction of the sCT. The axial, coronal, and sagittal slice predictions are rearranged to construct three distinct volumes. Subsequently, a median voting approach is adopted using the three volumes in order to enhance the final result.

number of filters at each step. In the decoder path, upsampling operations were performed before convolutional layers to restore feature maps to their original size, halving the number of filters at each step. Skip connections between the encoder and decoder paths facilitated the reuse of spatial information.

To train the aforementioned architecture, each client input 2D slices from each MRI in 3 anatomical planes, axial (Ax), coronal (Cor), and sagittal (Sag), as it is shown in Figure 4. Slices were presented to the network in a randomised order. After extracting all slices from each anatomical plane, they were shuffled to ensure that the DL model received non-sequential input from more than one anatomical plane at a time. This minimised the risk of the model becoming overly dependent on any single plane or orientation, encouraging comprehensive and plane-invariant feature learning across all planes [24].

3.4 Voting

As shown in Figure 5, in order to reconstruct the sCT, the predictions generated by the three anatomical planes were combined using a median voting approach to obtain the final voxel value, as proposed in [51]. This post-processing procedure ensured a more uniform and reliable output and was applied on both the server-side and the client-side predictions before the evaluation process. Specifically, once the predictions for each slice had been generated for each anatomical plane, the median result across the three axes was used to generate the final sCT voxel according to the formula [51]:

$$sHU_{V_n} = \text{median}(sHU_{\text{Cor}_n}; sHU_{\text{Ax}_n}; sHU_{\text{Sag}_n}), \quad n \in \{1, \dots, N\} \quad (1)$$

where V_n (with $n \in \{1, \dots, N\}$) refers to the pixel number, sHU refers to the synthetic Hounsfield Unit value of the n pixel for the coronal, axial, and sagittal sCT.

3.5 Aggregation strategy

After testing different aggregation strategies (see section 4.4.2), FedAvg in combination with FedProx to address the challenges associated with non-IID data across clients [29], was adopted for FedSynthCT-Brain.

More in detail, the weights from each client are aggregated round-by-round using a weighted average (thus, FedAvg), with each client’s contribution proportional to the size of its dataset.

$$w_{t+1} = \sum_{k=1}^K \frac{n_k}{n} w_{t+1}^k \quad (2)$$

where K represents the number of clients, n_k denotes the dataset size for client k , n is the total dataset size across all clients, and w_{t+1}^k are the weights of client k post-training.

As FedAvg underperform with non-IID data [32], FedProx was incorporated to address this limitation. The FedProx method, specifically designed for heterogeneous federated environment, introduces a proximal term $\frac{\mu}{2} \|w - w_t\|^2$ to the local objective function, penalising large deviations from the global model weights to control local update variations:

$$h_k(w, w_t) = F_k(w) + \frac{\mu}{2} \|w - w_t\|^2 \quad (3)$$

where $F_k(w)$ is the original local objective, w_t is the pre-training global model weight, w represents weights during local training, and μ is the proximal coefficient, within the range $[0, 1]$. Therefore, FedProx reduces update divergence and approximates FedAvg when $\mu = 0$ [29].

4 Experimental protocol

4.1 Data preprocessing details

The pre-processing pipeline used for each dataset can be divided into different steps, as shown in pseudo-code (Algorithm 1). To correct the bias field, the N4ITK algorithm [54] was employed. The algorithm was applied to each MRI with identical parameters.

Algorithm 1 Pre-processing pipeline for each Centre in pseudo-code

```

if Volume is MRI then
  Apply N4 Bias Field Correction
end if
if Volume Size > 256 × 256 × 256 then
  Apply Crop to centre the volume
  Resize to 256 × 256 × 256
end if
if Volume Size < 256 × 256 × 256 then
  Pad to 256 × 256 × 256
end if
if Volume is MRI then
  Apply Min-Max Normalization
end if

```

The second step was the standardisation of the anatomical axes orientation, which facilitates the application of the subsequent transforms and the extraction of slices. Then, all volumes that had a larger dimension than the target dimension were centred cropped to a size of $328 \times 256 \times 328$. Finally, all volumes were reshaped to a voxel size of $1mm \times 1mm \times 1mm$.

Furthermore, the resizing and padding process was executed by establishing a maximum dimension of 256 for all directions. The padding values were -1000 HU and 0 for CTs and MRIs, respectively.

Finally, the intensity values of each MRI were normalised to the $[0, 1]$ range using the Min-Max Normalization.

All experiments proposed in the subsequent sections were conducted with 4 clients, where each client used 2 patients for validation, 2 patients for testing, and the remaining for training.

4.2 Implementation and training settings

The implementation of the proposed work, was carried out in Python, using the Flower framework [5] for the FL infrastructure and the PyTorch [42] library for the DL implementation. To reproduce the federated environment and train the models, we used an NVIDIA A100 80GB GPU, 16 CPU cores, and 64GB of RAM from a Supermicro AS-4124GS-TNR 4U Rackmount GPU SuperServer.

To maintain consistency and prevent overfitting, a custom-built data augmentation pipeline was implemented for each client. The AugmentedDataLoader library⁴ was used to perform optimised on-the-fly data augmentation during training. In order to address the considerable computational demands associated with this data augmentation approach, two distinct data augmentation pipelines were employed: (i) a minimal pipeline, comprising a flip and a fixed-angle

⁴<https://github.com/ciroraggio/AugmentedDataLoader>

single-axis rotation; (ii) an extended pipeline, comprising a flip, a random-angle three-axis rotation and a fixed spatial translation; based on the amount of data available for the individual site.

A preliminary study was conducted to establish the optimal number of local epochs each client, thereby ensuring that the global model converged efficiently, rather than focusing exclusively on local optimisation. This involved an investigation into the impact of varying the number of local clients training epochs on the overall performance of the global model.

As reported in [29], it is beneficial to minimise the size of local updates in the context of FL. With this view, experiments were conducted using 1, 2, 3, and 5 epochs per round. It has been experimentally observed that an increasing number of epochs per round resulted in a proportional increase in computation time, with a degradation in image similarity metrics for the federated model. Consequently, the optimal number of local epochs was experimentally set to 1.

Each client model was trained using the Adam optimizer and the L1 loss. After an initial experimental analysis, the learning rate (LR) was set to 10^{-4} . The batch size was set to 32.

Each experiment ran for 30 rounds. This setup allowed for a rigorous and fair evaluation of both the model’s ability to generalise across rounds and its performance on unseen data.

4.3 Performance metrics

In order to evaluate the efficacy of the federated model both on the clients test datasets (centres A, B, C, and D), and unseen test dataset (centre E) standard image similarity metrics in the MRI to CT translation task were employed [49]. These included:

- Mean Absolute Error (MAE):

$$\text{MAE} = \frac{1}{n} \sum_{i=1}^n |CT_i - sCT_i|$$

where n is the total number of voxels in the region of interest.

- Structural Similarity Index Measure (SSIM) [49]:

$$\text{SSIM} = \frac{(2\mu_{sCT}\mu_{CT} + C_1)(2\sigma_{sCT,CT} + C_2)}{(\mu_{sCT}^2 + \mu_{CT}^2 + C_1)(\sigma_{sCT}^2 + \sigma_{CT}^2 + C_2)}$$

$$C_1 = (k_1L)^2, \quad C_2 = (k_2L)^2$$

$$\mu = \text{Mean}, \quad \sigma = \text{Variance/Covariance}$$

$$L = \text{Dynamic range}, \quad k_1 = 0.01, \quad k_2 = 0.03$$

- Peak Signal-to-Noise Ratio (PSNR) [49]:

$$\text{PSNR} = 10 \cdot \log \left(\frac{\text{MAX}_{CT}^2}{\text{MSE}} \right)$$

We further evaluated the efficiency using the time elapsed to complete a fixed number of rounds. This was aimed at identifying the most suitable architecture for the FL framework, balancing generalisation capability and training time. Indeed, minimizing training time is crucial, as extended training may exacerbate resource constraints, increase communication overhead among clients, and compromise the scalability of the system, particularly in multi-institutional collaborations [7].

4.4 Deep learning architecture and aggregation strategy selection

4.4.1 Deep learning architecture selection

We explored several variants of the U-Net architecture which has been used for centralised MRI-to-sCT-Simple U-Net [45], Spadea et al. U-Net [51], Fu et al. U-Net [13], Li et al. U-Nets [30]. These variants included variations in implementations, such as changes in network depth, feature map sizes, and the integration of attention mechanisms. Our analysis focused on evaluating the balance between computational complexity and generalization capability across these architectures.

Despite its inherent complexity, we also evaluated the winning DL model of the SynthRAD challenge, which used a patch-based approach for centralized MRI-to-sCT [21], namely the MSEP architecture [8]. To enable its use in

a FL context, we adapted the original implementation accordingly. To train the MSEP, patches with dimensions $48 \times 160 \times 160$ were extracted from each sample. The location of each patch was chosen randomly every epoch to increase the amount of possible training input data needed by intrinsic nature of the architecture. Since with this 3D DL approach, the model predicted overlapping patches and the number of predictions was not constant across the volume, the average value was calculated for each voxel using the median voting approach to reach a consensus. Given the computational complexity, the centres included in the federation were reduced to Centre A and Centre C.

The Adam optimizer with a learning rate of 2×10^{-4} was used. In this scenario, the hardware needed to lead the experiment was an NVIDIA A100 80GB GPU, 32 CPU cores, and 256GB of RAM from a Supermicro AS-4124GS-TNR 4U Rackmount GPU SuperServer.

4.4.2 Aggregation strategy selection

Once the most appropriate architecture was identified, a comparative analysis was conducted between the chosen aggregation strategy (i.e., FedAvg+FedProx), simple aggregation methods, such as FedAvg, and optimised and more complex techniques, such as FedYogi and FedAvgM with the incorporation of the momentum coefficient and the server-side learning rate.

Further optimisation was pursued through the incorporation of additional techniques, including FedBN and the combination of FedProx and FedBN, with the aim of refining and optimising the federated training process. This was done with a particular focus on ensuring that the global model could converge more rapidly and improve the robustness.

To determine the range of variability of the convergence trend within 25 rounds, the experiments were repeated 5 times for each strategy.

Regarding the hyper parameters used for each strategy, FedAvgM required the tuning of the momentum coefficient β and the server-side learning rate η_s . It was noted experimentally that the use of $\beta > 0.4$ and $\eta_s < 0.1$ leads to instability due to the inability of the model to reach the convergence. In light of this, the parameters used for FedAvgM were $\beta = 0.3$ and $\eta_s = 0.2$, respectively.

The FedYogi strategy necessitates the configuration and optimisation of different hyper parameters. These have been empirically optimised following a series of experiments with the objective of stabilising convergence. The best result for FedYogi was achieved with the following parameters: $\eta = 0.03$, $\eta_l = 10^{-4}$, $\beta_1 = 0.6$, $\beta_2 = 0.6$, and $\tau = 0.01$.

To add FedProx, different values of the proximal coefficient μ were tested. Higher μ corresponds to a greater penalty for significant deviations from the global model during local training, which may impede the model’s convergence. On the other hand, setting $\mu = 0$ would be equivalent to FedAvg. The optimal results for FedProx were obtained with a $\mu = 3$.

The FedBN approach was also tested with FedAvg and combined to FedAvg and FedProx. While no parameter tuning was required for FedBN, the conventional approach was modified.

Batch normalisation layers were excluded solely when transmitting the global model to clients, thereby enabling the aggregation of all layers, including batch normalization, at the server site. This alteration guarantees that the global model can leverage client-specific batch normalisation updates, enhancing its resilience when evaluated with previously unseen data.

5 Results

5.1 Benchmarking deep learning architectures

The performances of different state-of-the-art U-Nets, using a FL setup and the chosen aggregation strategy (FedAvg+FedProx), are presented in Table 2, in terms of median and inter-quartile range values of MAE, SSIM, and PSNR. The results are provided the test dataset of each centre participating to the federation (A, B, C, and D) and for the external centre E.

Image similarity assessment did not reveal any relevant difference across the tested U-Net architectures. However, when examining the total time required to complete 30 rounds, the U-Net architecture proposed by [34] required 12 hours and 34 minutes.

Table 3 presents the results of the MSEP training conducted in a federated setup. The experiment was completed in a total time of 85 hours and 37 minutes. It illustrates the time required for the federated training and the performance in terms of image similarity. This can be compared with the results obtained from 2D models to determine whether a 3D approach is a suitable candidate for this federated task.

Table 2: Comparison of the results obtained with different state-of-the-art U-Nets on the unseen centre dataset and federated centres (A, B, C, D) test data based on image similarity metrics and training time, considered as the total time to complete a fixed number of rounds.

	Method	MAE [HU]	SSIM	PSNR [dB]	Total Time
Centre A	Simple U-Net [45]	85.6 (84.8-86.4)	0.96 (0.96-0.96)	33.91 (33.65-34.18)	-
	Spadea et al.[51]	88.6 (88.0-89.3)	0.95 (0.95-0.95)	33.72 (33.45-33.99)	-
	Fu et al. [13]	91.3 (90.7-92.0)	0.95 (0.95-0.95)	33.43 (33.15-33.71)	-
	Li et al. (2020) [35]	93.0 (92.6-93.4)	0.95 (0.95-0.95)	33.34 (33.07-33.61)	-
	Li et al. (2019) [34]	89.7 (89.4-90.1)	0.95 (0.95-0.95)	33.64 (33.46-33.81)	-
Centre B	Simple U-Net [45]	126.1 (125.6-126.6)	0.86 (0.86-0.86)	21.83 (21.06-22.61)	-
	Spadea et al.[51]	128.6 (128.1-129.0)	0.86 (0.85-0.86)	21.81 (21.04-22.59)	-
	Fu et al. [13]	125.7 (124.8-126.7)	0.86 (0.86-0.86)	21.82 (21.04-22.61)	-
	Li et al. (2020) [35]	131.0 (130.5-131.5)	0.86 (0.85-0.86)	21.77 (21.01-22.54)	-
	Li et al. (2019) [34]	124.7 (124.4-125.1)	0.86 (0.86-0.86)	21.85 (21.08-22.63)	-
Centre C	Simple U-Net [45]	97.0 (94.1-99.9)	0.74 (0.71-0.77)	20.03 (19.36 - 20.71)	-
	Spadea et al.[51]	95.3 (92.0-98.6)	0.74 (0.71-0.77)	20.06 (19.37 - 20.73)	-
	Fu et al. [13]	89.1 (83.8-94.3)	0.74 (0.72-0.77)	20.05 (19.38 - 20.75)	-
	Li et al. (2020) [35]	97.1 (95.6-98.6)	0.74 (0.72-0.77)	20.03 (19.36 - 20.70)	-
	Li et al. (2019) [34]	92.9 (89.8-96.0)	0.74 (0.72-0.77)	20.05 (19.37 - 20.73)	-
Centre D	Simple U-Net [45]	70.8 (66.9-74.7)	0.93 (0.93-0.93)	27.05 (27.03-27.08)	-
	Spadea et al.[51]	71.7 (68.8-74.7)	0.93 (0.93-0.93)	27.05 (27.03-27.06)	-
	Fu et al. [13]	71.7 (68.4-75.0)	0.93 (0.93-0.93)	27.03 (27.01-27.05)	-
	Li et al. (2020) [35]	71.6 (66.5-76.7)	0.93 (0.93-0.93)	27.04 (27.00-27.07)	-
	Li et al. (2019) [34]	72.6 (63.4-76.8)	0.93 (0.93-0.93)	27.04 (27.02-27.06)	-
Centre E (Unseen)	Simple U-Net [45]	100.3 (94.5-108.2)	0.89 (0.86-0.89)	26.56 (25.53-27.52)	16h 22min
	Spadea et al.[51]	99.8 (92.6-108.9)	0.89 (0.86-0.89)	26.56 (25.53-27.52)	22h 41min
	Fu et al. [13]	99.8 (94.9-106.1)	0.89 (0.86-0.89)	26.61 (25.53-27.49)	20h 22min
	Li et al. (2020) [35]	98.9 (93.3-108.0)	0.89 (0.86-0.89)	26.55 (25.57-27.45)	15h 57min
	Li et al. (2019) [34]	102.0 (96.7-110.5)	0.89 (0.86-0.89)	26.58 (25.52-27.42)	12h 34min

Table 3: Results obtained on the test cases of the local clients (Centre A and C) and on the unseen dataset (Centre E) using the best performing 3D architecture (MSEP) of the SynthRAD2023 challenge for the head MRI to sCT task, as a federated model.

	MAE [HU]	SSIM	PSNR [dB]	Total Time
Centre A	229.9 (196.3-232.6)	0.86 (0.86-0.87)	26.56 (26.45-27.83)	-
Centre C	219.5 (213.4-231.0)	0.65 (0.59-0.71)	18.98 (18.02-20.09)	-
Centre E (Unseen)	240.5 (220.7-250.7)	0.79 (0.77-0.80)	23.70 (23.09-24.29)	85h 37min

Table 4: Results obtained for the tested aggregation strategies in terms of image similarity and the number of rounds required to achieve the best result. The mean and standard deviation (Std) are presented for both rounds and the Mean Absolute Error (MAE).

Strategy	Metric	Experiment					Mean±Std
		1	2	3	4	5	
FedAvg	Round	10	16	20	10	18	14.8 ± 4.1
	MAE [HU]	99.5	99.3	100.8	102.6	101.1	100.7 ± 1.4
FedAvgM	Round	28	27	28	29	27	27.8 ± 0.7
	MAE [HU]	102	101.8	103	101	101.4	101.8 ± 0.7
FedYogi	Round	13	13	17	4	12	11.8 ± 4.3
	MAE [HU]	207.7	230.6	225.9	236.1	234.4	226.9 ± 10.2
FedAvg + FedBN	Round	20	6	15	21	21	16.6 ± 5.7
	MAE [HU]	101.0	100.9	99.6	100.7	98.3	100.1 ± 1.1
FedAvg + FedProx + FedBN	Round	15	8	15	21	19	15.6 ± 4.4
	MAE [HU]	99.2	99.9	97.5	100.1	100.1	99.36 ± 1
FedAvg + FedProx (Our)	Round	18	8	14	14	9	12.6 ± 3.7
	MAE [HU]	99.8	99.2	100.1	101.6	98.3	99.8 ± 1.1

5.2 Benchmarking aggregation strategies

Table 4 presents the best result obtained for each aggregation strategy, tested on the unseen dataset (centre E). Results are reported in terms of MAE, which resulted the most sensitive image similarity metric in the benchmarking of DL architectures. The experiments (Experiment 1, 2, 3, 4, 5), were repeated 5 times for each strategy to determine the range of variability of the convergence trend within 25 rounds. This comparison helps to understand which aggregation strategy gives the best result in a stable and efficient way. For each experiment, the number of rounds performed to obtain the best result is also reported.

5.3 Federated sCTs

As reported in Table 2, using the U-Net by Li et al. [34] and FedAvg combined with FedProx as aggregation strategy, the median MAE (inter-quartile range) for the unseen dataset was 102.0 HU (96.7 – 110.5 HU).

Figure 6 shows results for the best and worst cases of Centre E.

A view of the central slice in the three anatomical places is provided, demonstrating the advantages and limitations of the framework. Furthermore, the difference between the ground truth CT and the sCT is shown to assess critical pattern in the sCT generation.

The results obtained by the federated model on one random patient of each client test dataset are also presented for each centre in Figures 7 and 8. The central slice of the three anatomical planes is provided for the clients' data, along with the ground truth CT and sCT difference. The figures include rectangles of different colours to identify errors or artefacts observed in the images during the comparative analysis, that are not evident when considering only the similarity metrics.

6 Discussion

This study addressed the challenges of bias and limited diversity in medical imaging datasets caused by single-institution reliance in the context of MRI-to-sCT. Our proposal was to introduce a FL framework designed for MRI-to-CT synthesis in brain imaging, FedSynthCT-Brain. We reproduced a realistic FL environment, adhering to all FL principles, using a cross-silo horizontal FL paradigm to enable the collaborative training of DL models as if multiple institutions were involved. To further validate the effectiveness of our approach, we tested the performance of the federated model on an unseen dataset, demonstrating its generalisability to external heterogeneous data sources.

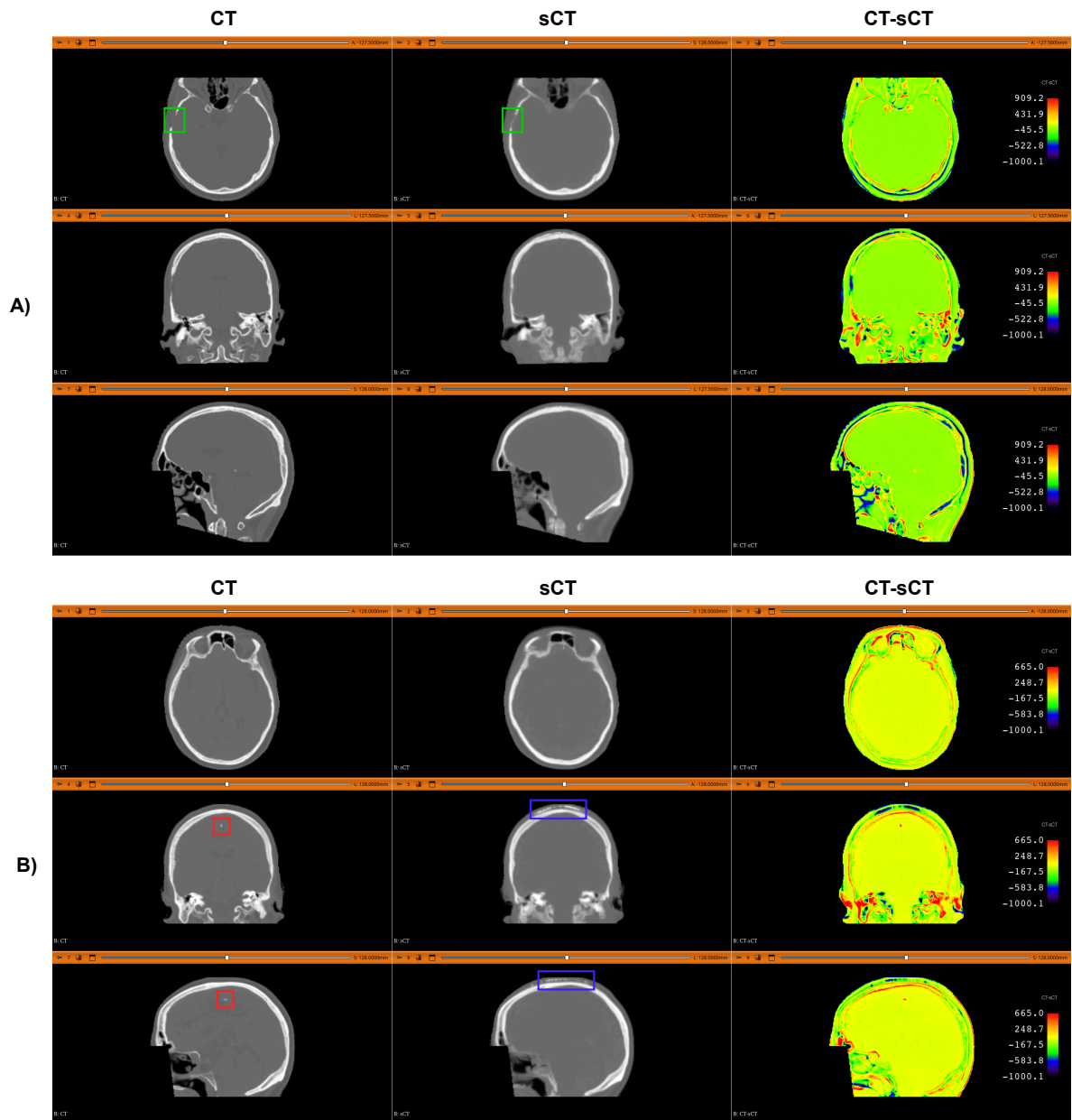


Figure 6: The figure shows the centre slice for the axial, coronal and sagittal planes, which is used for an evaluation of the worst and best –A and B respectively– predictions based on image similarity metrics of the federated model on the unseen dataset (Centre E). In the case B, the red square highlights a calcification in the ground truth CT, which is not correctly predicted by the model. In the case B, the blue rectangle also highlights a thin duplication of the upper skull bone. This issue has been identified exclusively within the predictions generated by the federated model on the Centre E dataset. The colour map on the left illustrates the differences between the CT and the sCT, highlighting regions where the model exhibits a higher or lower tendency to over or underestimate the actual outcome.

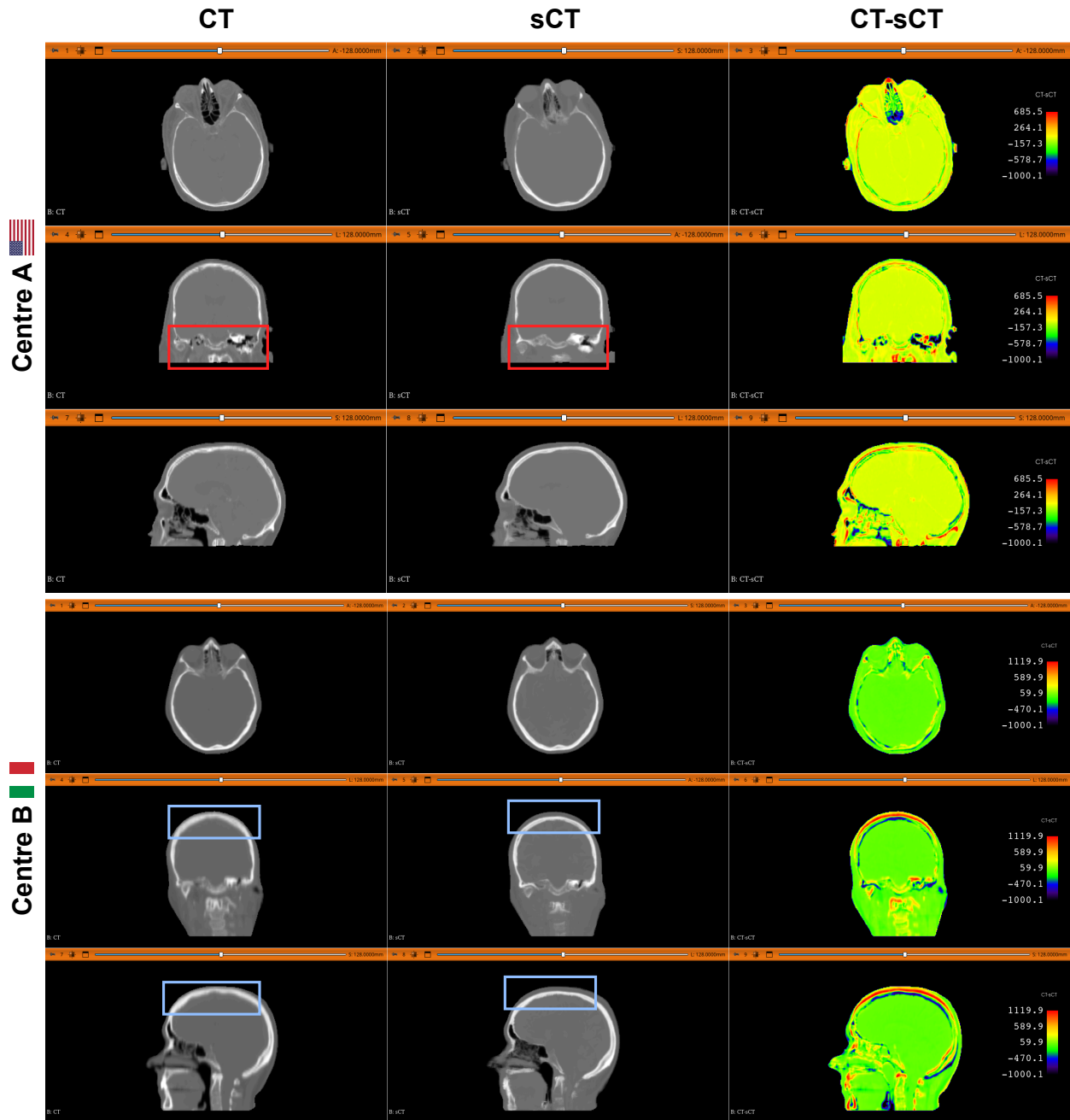


Figure 7: The figure shows the central slice for the axial, coronal, and sagittal planes, which is used for an assessment of one of the two test cases of Centres A and B, respectively. The red boxes in the Centre A-coronal view-comparison highlight the approximation of the small structure performed by the model during the sCT generation. The blue boxes in the Centre B-coronal and sagittal views-comparison indicate the presence of an artefact in the ground truth CT, whereby the upper part is larger than expected. Despite this artefact, the federated model predicts a smaller skull structure, and thus a more realistic outcome.

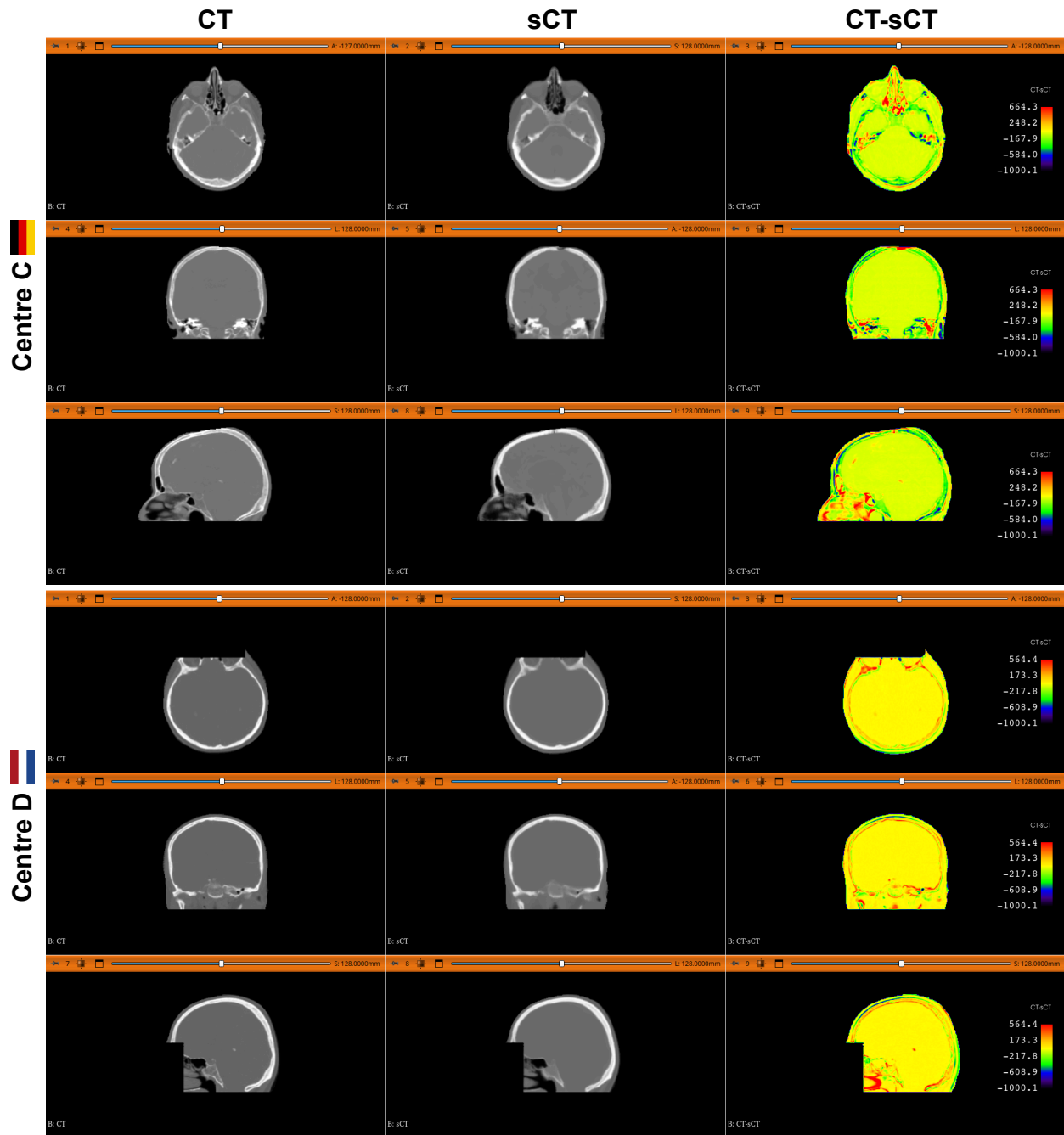


Figure 8: The results obtained from the federated model for one of the two test cases of Centres C and D. As for the other Centres of the federation, conversion problems emerge in small and detailed areas, while for the majority of the image composed of soft tissue the error remains contained.

Regarding the evaluation of U-Net architectures, the results obtained on Centre E — the unseen dataset — as well as across the various Centres in the federation, reveal no relevant differences in image similarity metrics when comparing different architectures. Based on the MAE metric, the minimal variation in HU does not allow for the identification of a clearly superior U-Net design. This could imply that, within the context of the FedSynthCT-Brain framework, the architectures are sufficiently robust to handle the data variability across the different centres. Consequently, the focus shifted to evaluating the disparity in efficiency among the different implementations, as this becomes a critical factor in determining the most suitable model for FL applications.

Referring to results about the time taken to complete the experiment for a fixed number of rounds (Total Time, see Table 2), the U-Net proposed by Li et al. [34] was the most efficient. These findings are relevant in federated environments, where limited computational resources and the time spent on computation become major factors. Consequently, a model that requires less time to be trained and federated, might mitigate interruptions in the communication during training and minimise synchronisation times.

We also integrated the winning MSEP architecture from the SynthRAD2023 challenge into our FL framework by adapting its original 3D implementation. Despite efforts to reduce computational overhead — such as limiting the number of participating clients and reducing the size of the 3D patches — the time required for a single federated round remained prohibitively high. Specifically, one round took approximately 85 hours and 37 minutes, compared to just 49 minutes for the U-Net model proposed by Li et al. [34]. Moreover, the federated MSEP architecture’s performance fell short when compared to its centralised counterpart. This decline can be primarily attributed to: (i) the adjustments made to the training pipeline to accommodate the federated framework, and (ii) the reduced number of rounds and clients necessitated by the computational complexity of the 3D approach.

Moving to the aggregation strategies, the analysis of FedAvg results (see Table 4, revealed that the optimal performance were obtained in 25 rounds, exhibiting minimal variation – 1.4 HU – in terms of MAE. However, when compared to the proposed aggregation method (FedAvg+FedProx), FedAvg required an average higher number of rounds, indicating a longer time to reach its optimal result. Referring to the Table 4, using FedProx enhances the performance of FedAvg and accelerates the convergence process, achieving its optimal result in an average of 12.6 ± 3.7 rounds, compared to 14.8 ± 4.1 rounds for the FedAvg alone. This finding aligns with previous studies in closer fields of research (e.g., [33]), which highlight that the introduction of a proximal term can mitigate the impact of client heterogeneity and improve convergence stability in FL settings.

Despite the introduction of the momentum coefficient and the server-side learning rate, the FedAvgM strategy was unable to improve the performance in terms of image similarity. Also in this case, a minimal stochastic variation in terms of MAE was observed. As illustrated in both Figure 10 and Table 4, while the trend of convergence remains consistent across experiments, FedAvgM requires 27.8 ± 0.7 (mean \pm std) rounds, thereby doubling the number of rounds to achieve the optimal result in comparison to the proposed aggregation strategy. Consequently, it can be deduced that the momentum coefficient and the server-side learning rate do not offer any advantages in terms of performance or image quality when compared to the proposed method. Similar challenges with FedAvgM have been reported in [44], where the additional hyperparameters introduced by momentum strategies were found to complicate tuning without consistently improving performance.

The more complex and optimised strategy FedYogi, presented several stability problems in the performed experiments. Despite the efforts made to tune the hyper-parameters of the strategy, it did not yield comparable or acceptable results compared to simpler strategies, as evidenced by the average MAE of 226.9 ± 10.2 .

From Table 4, a delay in the convergence of the simpler FedAvg has been noted when introducing FedBN, in contrast to the approach of combining only FedProx.

To confirm the benefit of the proximal term in this specific federated task, a combination of FedProx with FedAvg and FedBN (FedAvg + FedProx + FedBN) was investigated. It is evident from Table 4 that, despite the lack of improvement, the introduction of the proximal term (FedProx) resulted in a slight reduction in the average number of rounds required for convergence. Consequently, we concluded that the chosen strategy, which involves the simple combination of FedAvg with FedProx, with a proximal coefficient $\mu = 3$, offers a comparable performance to more complex and optimised strategies, while requiring fewer rounds.

As in the case of the U-Nets evaluation, our findings reaffirm previous insights into the balance between model efficiency and efficacy [29] while highlighting opportunities for future exploration, particularly in aggregation strategies that improve robustness and resource efficiency in FL scenarios.

Regarding the generalisation ability of the federated model, the evaluation of CT and sCT similarity on the unseen dataset (see Figure 6) revealed that for the predominant portion of the image, specifically the soft tissue, the discrepancy

ranges between -100 HU and 100 HU, with peak errors occurring in specific and limited regions, such as the nasal and oral cavities.

Some inconsistencies were identified in the upper skull of a few patients, indicated by the blue box in Figure 6, case B). The wrong I2I translation produced a subtle bone mirroring. In other cases the federated model was not able to predict the presence of calcifications in the brain tissue. This failure can be attributed to the limited number of examples that exhibited this brain calcification in the federation, which precluded the model from identifying abnormal cases such as the one highlighted.

Despite the Centre E's dataset being external to the training, the federated model demonstrated its capacity to predict a missing portion of bone in the axial view (see Figure 6, case A, green box).

The results of the individual centres presented in Figure 7 and Figure 8, exhibited various advantages and disadvantages, given the differing characteristics of the data from each Centre.

In Figure 7 the aforementioned issue identified in the upper part of the skull for some cases of the Centre E does not occur. However, the smaller and more detailed areas tended to be approximated, resulting in a loss of detail, particularly in the proximity of the nasal cavities, as can be note within the red box provided in the coronal view for the test case of the centre A.

As described in Section 3.1, Centre B was introduced in the federation to increase data heterogeneity, as the MRIs were acquired with a hybrid PET-MRI scanner, with larger CT slice thickness and different X-ray tube energy (120 kV vs. 140 kV). From Table 2, it is evident that the error for the Centre B is greater than for the other clients, emphasising the difference from the other images in the federation. However, it can be observed that the error is partly due to the lower spatial resolution of the ground truth CT, introducing partial volume artefacts in the upper part of the skull (see Figure 7, light blue box). The result of this artefact is a noticeable, unrealistic thickening of the bone, as presented in Figure 9. Despite this problem, the skull bone of the predicted federated sCT appears more realistic and consistent with other examples. This establishes an advantage of the federation, as the influence given by the weights of the other Centres allows the federated model to remain robust in front of optimization errors during training.

In Figure 8, results obtained for Centres C and D test cases are presented. The limitations of the model in reconstructing small, detailed parts are also evident in these cases. However, from the difference shown on the left, it can be observed that the error for the largest part of the images is always in the [-100,100] HU range, while the highest errors are consistently present in the proximity of the air and detailed zones.

This work established the foundations for future developments. A possible improvement could involve optimizing the implementation of 3D architectures for federated scenarios by leveraging more efficient training strategies, such as model pruning, knowledge distillation, or dimensionality reduction [48]. Additionally, exploring hybrid federated approaches, such as cross-silo horizontal FL with asynchronous updates or client clustering [40, 57], could reduce synchronization times.

Moreover, the implementation of specific pre-processing or data harmonisation techniques can be considered to enhance the homogeneity of the data and to mitigate potential hidden artefacts. This, consequently, will improve the quality of the sCTs for both the Centres within the federation and in the generalisation task.

7 Conclusion

We proposed, for the first time to best of our knowledge, a FL approach for MRI to sCT, with a specific focus on the brain region. Despite the intrinsic complexity of the task, which was evaluated including real clinical datasets. The results illustrate the potential of this methodology to safeguard patient confidentiality while sustaining robust model performance. The incorporation of additional clinics and institutions into the federation will enhance the accessibility of diverse and heterogeneous data, thereby optimising the model's generalisability and performance in a secure and scalable manner. This approach allows for the creation of a model with the capacity to generalise to previously unseen datasets, which is a crucial aspect for wider clinical applicability. Furthermore, it underscores the viability of federated learning as a sustainable solution for medical imaging tasks.

Apart from the advantages that have been highlighted, the objective of this work was to establish the foundations for future research. Multiple approaches can be followed to enhance the final outcome and progressively reduce the necessity for data centralisation and the training of individual models for each clinic. Future developments will include dosimetric studies to establish whether the results obtained can be used also in the clinical environment for external beam radiotherapy and targeted radionuclide treatments, as well as the benchmarking of aggregation methods that extend beyond classical methodologies but necessitate additional effort for implementation, such as FedFisher [22] and

FedDG [36]. Furthermore, efforts will be made to integrate and optimise recent sCT methods employing complex 3D architectures.

Data availability

The data used for the study acquired from centre A, B and C are confidential. The data from Centre D and Centre E were extracted from the public SynthRAD2023 Grand Challenge dataset and are available at <https://synthrad2023.grand-challenge.org/>.

Acknowledgments

We would like to acknowledge Dr. C. Catana (Massachusetts General Hospital) for contributing to data sharing and support during this research.

A Centre B artefact measurement

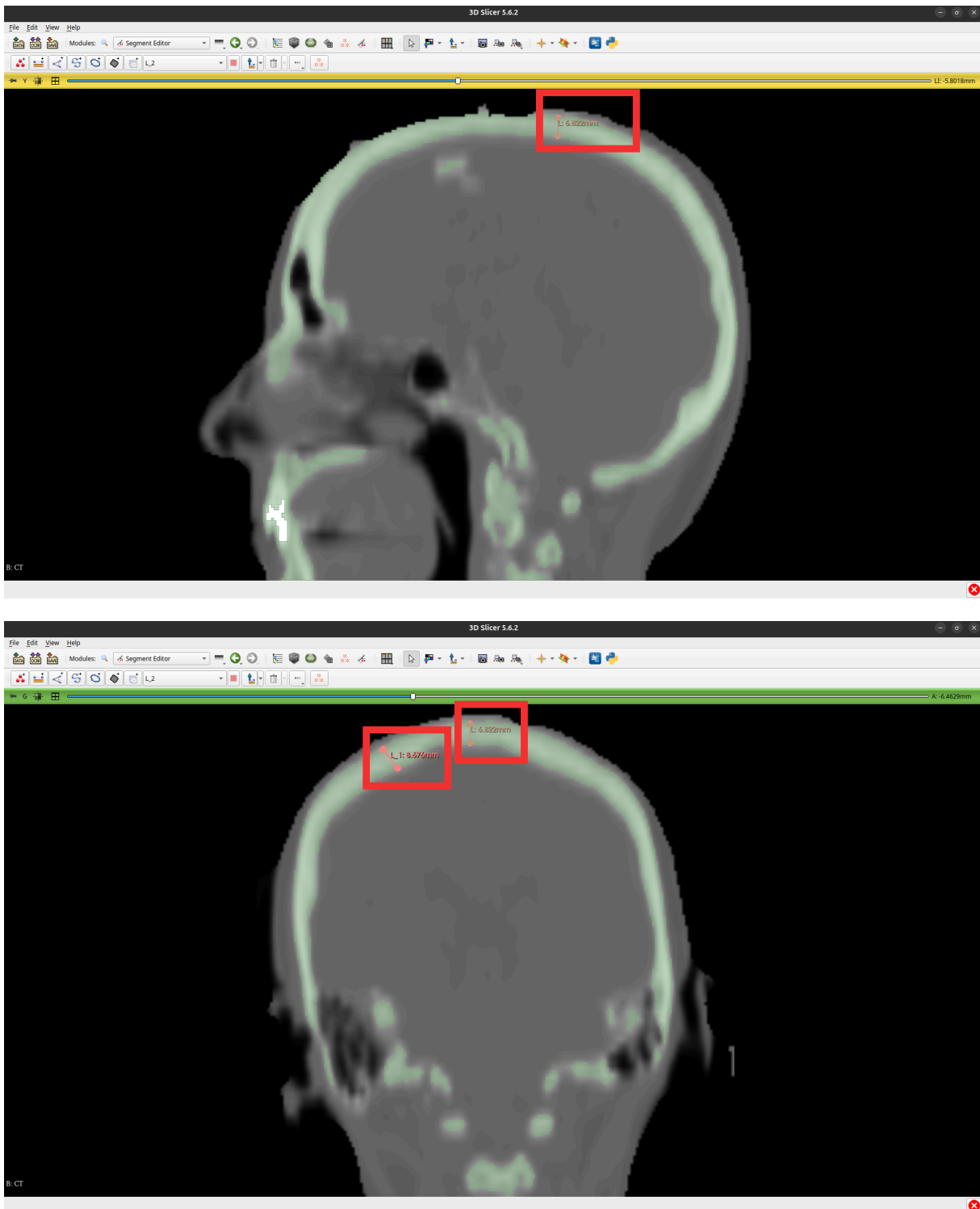


Figure 9: Measurement of a portion of the skull to highlight the partial volume artefact due to the higher slice thickness in Centre B CTs.

B Aggregation strategies convergence trends

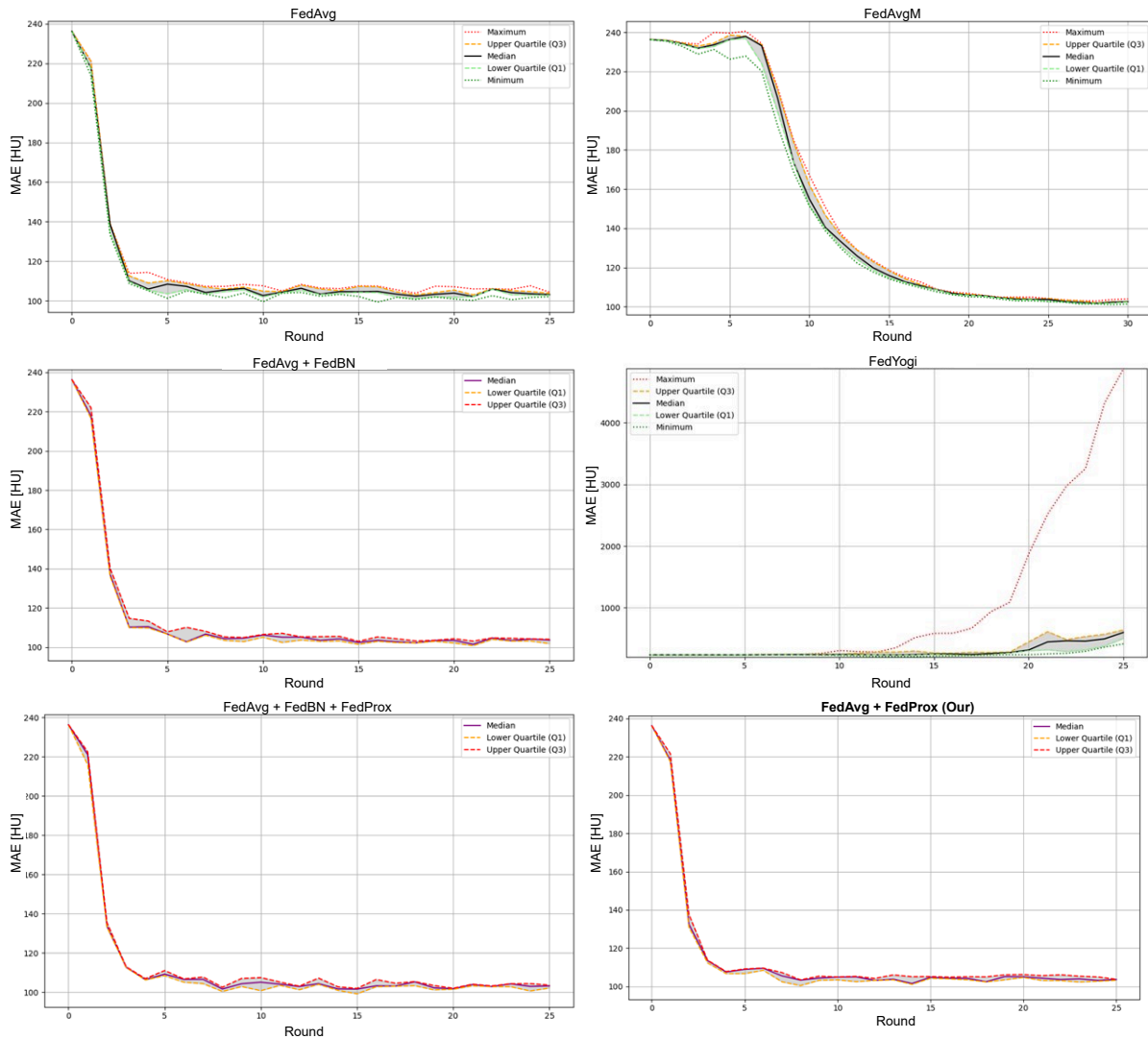


Figure 10: Comparison of convergence trends of aggregation strategies.

References

- [1] M. Adnan, S. Kalra, J. C. Cresswell, G. W. Taylor, and H. R. Tizhoosh. Federated learning and differential privacy for medical image analysis. *Scientific reports*, 12(1):1953, 2022.
- [2] E. Albalawi, M. T.R., A. Thakur, V. V. Kumar, M. Gupta, S. B. Khan, and A. Almusharraf. Integrated approach of federated learning with transfer learning for classification and diagnosis of brain tumor. *BMC Medical Imaging*, Jun 2024.
- [3] R. S. Antunes, C. André da Costa, A. Küderle, I. A. Yari, and B. Eskofier. Federated learning for healthcare: Systematic review and architecture proposal. *ACM Transactions on Intelligent Systems and Technology (TIST)*, 13(4):1–23, 2022.

- [4] M. A. Bahloul, S. Jabeen, S. Benoumhani, H. A. Alsaleh, Z. Belkhatir, and A. Al-Wabil. Advancements in synthetic ct generation from mri: A review of techniques, and trends in radiation therapy planning. *Journal of Applied Clinical Medical Physics*, 25(11), Sep 2024.
- [5] D. J. Beutel, T. Topal, A. Mathur, X. Qiu, J. Fernandez-Marques, Y. Gao, L. Sani, K. H. Li, T. Parcollet, P. P. B. de Gusmão, and N. D. Lane. Flower: A friendly federated learning research framework, 2022.
- [6] Q. Chang, H. Qu, Y. Zhang, M. Sabuncu, C. Chen, T. Zhang, and D. Metaxas. Synthetic learning: Learn from distributed asynchronized discriminator gan without sharing medical image data, 2020.
- [7] X. Chen, X. Zhou, H. Zhang, M. Sun, and T. Zhao. Cost-effective federated learning: A unified approach to device and training scheduling. In *ICC 2024-IEEE International Conference on Communications*, pages 3488–3493. IEEE, 2024.
- [8] Z. Chen, K. Zheng, C. Li, and Z. Yiwen. A hybrid network with multi-scale structure extraction and preservation for mr-to-ct synthesis in synthrad2023. *SynthRAD2023*, 2023.
- [9] O. Dalmaz, M. U. Mirza, G. Elmas, M. Özbek, S. U. Dar, E. Ceyani, K. K. Oguz, S. Avestimehr, and T. Çukur. One model to unite them all: Personalized federated learning of multi-contrast mri synthesis. *Medical Image Analysis*, 94:103121, 2024.
- [10] S. Dayarathna, K. T. Islam, S. Uribe, G. Yang, M. Hayat, and Z. Chen. Deep learning based synthesis of mri, ct and pet: Review and analysis. *Medical Image Analysis*, 92:103046, 2024.
- [11] A. Fedorov, R. Beichel, J. Kalpathy-Cramer, J. Finet, J.-C. Fillion-Robin, S. Pujol, C. Bauer, D. Jennings, F. Fennessy, M. Sonka, J. Buatti, S. Aylward, J. V. Miller, S. Pieper, and R. Kikinis. 3d slicer as an image computing platform for the quantitative imaging network. *Magnetic Resonance Imaging*, 30(9):1323–1341, 2012. Quantitative Imaging in Cancer.
- [12] I. Feki, S. Ammar, Y. Kessentini, and K. Muhammad. Federated learning for covid-19 screening from chest x-ray images. *Applied Soft Computing*, 106:107330, 2021.
- [13] J. Fu, Y. Yang, K. Singhraj, D. Ruan, F.-I. Chu, D. A. Low, and J. H. Lewis. Deep learning approaches using 2d and 3d convolutional neural networks for generating male pelvic synthetic computed tomography from magnetic resonance imaging. *Medical Physics*, 46(9):3788–3798, 2019.
- [14] R. Graf, J. Schmitt, S. Schlaeger, H. K. Möller, V. Sideri-Lampretsa, A. Sekuboyina, S. M. Krieg, B. Wiestler, B. Menze, D. Rueckert, and J. S. Kirschke. Denoising diffusion-based mri to ct image translation enables automated spinal segmentation. *European Radiology Experimental*, 7(1):70, Nov 2023.
- [15] J. Grigo, J. Szkitsak, D. Höfler, R. Fietkau, F. Putz, and C. Bert. “sct-feasibility” - a feasibility study for deep learning-based mri-only brain radiotherapy. *Radiation Oncology*, 19(1):33, Mar 2024.
- [16] H. Guan, P.-T. Yap, A. Bozoki, and M. Liu. Federated learning for medical image analysis: A survey. *Pattern Recognition*, page 110424, 2024.
- [17] N. Hernandez-Cruz, P. Saha, M. M. K. Sarker, and J. A. Noble. Review of federated learning and machine learning-based methods for medical image analysis. *Big Data and Cognitive Computing*, 8(9), 2024.
- [18] M. N. Hossen, V. Panneerselvam, D. Koundal, K. Ahmed, F. M. Bui, and S. M. Ibrahim. Federated machine learning for detection of skin diseases and enhancement of internet of medical things (iomt) security. *IEEE Journal of Biomedical and Health Informatics*, 27(2):835–841, 2023.
- [19] S.-H. Hsu, Z. Han, J. E. Leeman, Y.-H. Hu, R. H. Mak, and A. Sudhyadhom. Synthetic ct generation for mri-guided adaptive radiotherapy in prostate cancer. *Frontiers in Oncology*, 12, 2022.
- [20] E. M. Huijben, M. L. Terpstra, A. J. Galapon, S. Pai, A. Thummerer, P. Koopmans, M. Afonso, M. van Eijnatten, O. Gurney-Champion, Z. Chen, Y. Zhang, K. Zheng, C. Li, H. Pang, C. Ye, R. Wang, T. Song, F. Fan, J. Qiu, Y. Huang, J. Ha, J. Sung Park, A. Alain-Beaudoin, S. Bériault, P. Yu, H. Guo, Z. Huang, G. Li, X. Zhang, Y. Fan, H. Liu, B. Xin, A. Nicolson, L. Zhong, Z. Deng, G. Müller-Franzes, F. Khader, X. Li, Y. Zhang, C. Hémon, V. Boussot, Z. Zhang, L. Wang, L. Bai, S. Wang, D. Mus, B. Kooiman, C. A. Sargeant, E. G. Henderson, S. Kondo, S. Kasai, R. Karimzadeh, B. Ibragimov, T. Helfer, J. Dafflon, Z. Chen, E. Wang, Z. Perko, and M. Maspero. Generating synthetic computed tomography for radiotherapy: Synthrad2023 challenge report. *Medical Image Analysis*, 97:103276, 2024.
- [21] E. M. Huijben, M. L. Terpstra, S. Pai, A. Thummerer, P. Koopmans, M. Afonso, M. van Eijnatten, O. Gurney-Champion, Z. Chen, Y. Zhang, et al. Generating synthetic computed tomography for radiotherapy: Synthrad2023 challenge report. *Medical image analysis*, 97:103276, 2024.
- [22] D. Jhunjhunwala, S. Wang, and G. Joshi. Fedfisher: Leveraging fisher information for one-shot federated learning, 2024.

- [23] G. A. Kaissis, M. R. Makowski, D. Rückert, and R. F. Braren. Secure, privacy-preserving and federated machine learning in medical imaging. *Nature Machine Intelligence*, 2(6):305–311, 2020.
- [24] K. Kamnitsas, C. Ledig, V. F. Newcombe, J. P. Simpson, A. D. Kane, D. K. Menon, D. Rueckert, and B. Glocker. Efficient multi-scale 3d cnn with fully connected crf for accurate brain lesion segmentation. *Medical image analysis*, 36:61–78, 2017.
- [25] H. Koh, T. Y. Park, Y. A. Chung, J.-H. Lee, and H. Kim. Acoustic simulation for transcranial focused ultrasound using gan-based synthetic ct. *IEEE Journal of Biomedical and Health Informatics*, 26(1):161–171, 2022.
- [26] Y. Lei, J. Harms, T. Wang, Y. Liu, H.-K. Shu, A. B. Jani, W. J. Curran, H. Mao, T. Liu, and X. Yang. MRI-only based synthetic CT generation using dense cycle consistent generative adversarial networks. *Med Phys*, 46(8):3565–3581, June 2019.
- [27] D. Li, A. Kar, N. Ravikumar, A. F. Frangi, and S. Fidler. Fed-sim: Federated simulation for medical imaging, 2020.
- [28] G. Li, L. Bai, C. Zhu, E. Wu, and R. Ma. A novel method of synthetic ct generation from mr images based on convolutional neural networks. In *2018 11th International Congress on Image and Signal Processing, BioMedical Engineering and Informatics (CISP-BMEI)*, pages 1–5, 2018.
- [29] T. Li, A. K. Sahu, M. Zaheer, M. Sanjabi, A. Talwalkar, and V. Smith. Federated optimization in heterogeneous networks. *Proceedings of Machine learning and systems*, 2:429–450, 2020.
- [30] T. Li, M. Sanjabi, A. Beirami, and V. Smith. Fair resource allocation in federated learning, 2020.
- [31] W. Li, F. Milletari, D. Xu, N. Rieke, J. Hancox, W. Zhu, M. Baust, Y. Cheng, S. Ourselin, M. J. Cardoso, and A. Feng. Privacy-preserving federated brain tumour segmentation, 2019.
- [32] X. Li, K. Huang, W. Yang, S. Wang, and Z. Zhang. On the convergence of fedavg on non-iid data. *arXiv preprint arXiv:1907.02189*, 2019.
- [33] X. Li, M. Jiang, X. Zhang, M. Kamp, and Q. Dou. FedBN: Federated learning on non-iid features via local batch normalization. *arXiv preprint arXiv:2102.07623*, 2021.
- [34] Y. Li, W. Li, P. He, J. Xiong, J. Xia, and Y. Xie. Ct synthesis from mri images based on deep learning methods for mri-only radiotherapy. In *2019 International Conference on Medical Imaging Physics and Engineering (ICMIPE)*, pages 1–6, 2019.
- [35] Y. Li, W. Li, J. Xiong, J. Xia, and Y. Xie. Comparison of supervised and unsupervised deep learning methods for medical image synthesis between computed tomography and magnetic resonance images. *BioMed Research International*, 2020(1):5193707, 2020.
- [36] Q. Liu, C. Chen, J. Qin, Q. Dou, and P.-A. Heng. Feddg: Federated domain generalization on medical image segmentation via episodic learning in continuous frequency space, 2021.
- [37] Y. Liu, A. Chen, H. Shi, S. Huang, W. Zheng, Z. Liu, Q. Zhang, and X. Yang. Ct synthesis from mri using multi-cycle gan for head-and-neck radiation therapy. *Computerized Medical Imaging and Graphics*, 91:101953, 2021.
- [38] Y. Liu, G. Luo, and Y. Zhu. Fedfms: Exploring federated foundation models for medical image segmentation. In M. G. Linguraru, Q. Dou, A. Feragen, S. Giannarou, B. Glocker, K. Lekadir, and J. A. Schnabel, editors, *Medical Image Computing and Computer Assisted Intervention – MICCAI 2024*, pages 283–293, Cham, 2024. Springer Nature Switzerland.
- [39] J. Lo, T. T. Yu, D. Ma, P. Zang, J. P. Owen, Q. Zhang, R. K. Wang, M. F. Beg, A. Y. Lee, Y. Jia, and M. V. Sarunic. Federated learning for microvasculature segmentation and diabetic retinopathy classification of oct data. *Ophthalmology Science*, 1(4):100069, 2021.
- [40] J. Nguyen, K. Malik, H. Zhan, A. Yousefpour, M. Rabbat, M. Malek, and D. Huba. Federated learning with buffered asynchronous aggregation. In *International Conference on Artificial Intelligence and Statistics*, pages 3581–3607. PMLR, 2022.
- [41] M. Özbey, O. Dalmaz, S. U. Dar, H. A. Bedel, Ş. Öztürk, A. Güngör, and T. Çukur. Unsupervised medical image translation with adversarial diffusion models. *IEEE Transactions on Medical Imaging*, 42(12):3524–3539, 2023.
- [42] A. Paszke, S. Gross, F. Massa, A. Lerer, J. Bradbury, G. Chanan, T. Killeen, Z. Lin, N. Gimelshein, L. Antiga, A. Desmaison, A. Köpf, E. Yang, Z. DeVito, M. Raison, A. Tejani, S. Chilamkurthy, B. Steiner, L. Fang, J. Bai, and S. Chintala. *PyTorch: an imperative style, high-performance deep learning library*. Curran Associates Inc., 2019.

- [43] L. Qiu, J. Cheng, H. Gao, W. Xiong, and H. Ren. Federated semi-supervised learning for medical image segmentation via pseudo-label denoising. *IEEE Journal of Biomedical and Health Informatics*, 27(10):4672–4683, 2023.
- [44] S. Reddi, Z. Charles, M. Zaheer, Z. Garrett, K. Rush, J. Konečný, S. Kumar, and H. B. McMahan. Adaptive federated optimization. *arXiv preprint arXiv:2003.00295*, 2020.
- [45] O. Ronneberger, P. Fischer, and T. Brox. U-net: Convolutional networks for biomedical image segmentation. In N. Navab, J. Hornegger, W. M. Wells, and A. F. Frangi, editors, *Medical Image Computing and Computer-Assisted Intervention – MICCAI 2015*, pages 234–241, Cham, 2015. Springer International Publishing.
- [46] S. S. Sandhu, H. T. Gorji, P. Tavakolian, K. Tavakolian, and A. Akhbardeh. Medical imaging applications of federated learning. *Diagnostics*, 13(19), 2023.
- [47] M. J. Sheller, G. A. Reina, B. Edwards, J. Martin, and S. Bakas. Multi-Institutional deep learning modeling without sharing patient data: A feasibility study on brain tumor segmentation. *Brainlesion*, 11383:92–104, Jan. 2019.
- [48] S. Soni, A. Saeed, and Y. M. Asano. Federated learning with a single shared image. In *Proceedings of the IEEE/CVF Conference on Computer Vision and Pattern Recognition*, pages 7782–7790, 2024.
- [49] M. F. Spadea, M. Maspero, P. Zaffino, and J. Seco. Deep learning based synthetic-ct generation in radiotherapy and pet: A review. *Medical Physics*, 48(11):6537–6566, 2021.
- [50] M. F. Spadea, G. Pileggi, P. Zaffino, P. Salome, C. Catana, D. Izquierdo-Garcia, F. Amato, and J. Seco. Deep convolution neural network (dcnn) multiplane approach to synthetic ct generation from mr images - application in brain proton therapy. *International Journal of Radiation Oncology, Biology, Physics*, 105(3):495–503, Nov 2019.
- [51] M. F. Spadea, G. Pileggi, P. Zaffino, P. Salome, C. Catana, D. Izquierdo-Garcia, F. Amato, and J. Seco. Deep convolution neural network (dcnn) multiplane approach to synthetic ct generation from mr images—application in brain proton therapy. *International Journal of Radiation Oncology, Biology, Physics*, 105(3):495–503, 2019.
- [52] A. Thummerer, P. Zaffino, M. F. Spadea, A. Knopf, and M. Maspero. Artificial intelligence to generate synthetic ct for adaptive particle therapy. In *Imaging in Particle Therapy*, 2053-2563, pages 8–1 to 8–16. IOP Publishing, 2024.
- [53] A. Tuladhar, L. Tyagi, R. Souza, and N. D. Forkert. Federated learning using variable local training for brain tumor segmentation. In A. Crimi and S. Bakas, editors, *Brainlesion: Glioma, Multiple Sclerosis, Stroke and Traumatic Brain Injuries*, pages 392–404, Cham, 2022. Springer International Publishing.
- [54] N. J. Tustison, B. B. Avants, P. A. Cook, Y. Zheng, A. Egan, P. A. Yushkevich, and J. C. Gee. N4ITK: improved N3 bias correction. *IEEE Trans Med Imaging*, 29(6):1310–1320, Apr. 2010.
- [55] J. Wang, Y. Jin, D. Stoyanov, and L. Wang. Feddp: Dual personalization in federated medical image segmentation. *IEEE Transactions on Medical Imaging*, 43(1):297–308, 2024.
- [56] J. Wang, G. Xie, Y. Huang, J. Lyu, F. Zheng, Y. Zheng, and Y. Jin. Fedmed-gan: Federated domain translation on unsupervised cross-modality brain image synthesis. *Neurocomputing*, 546:126282, 2023.
- [57] Z. Wang, H. Xu, J. Liu, Y. Xu, H. Huang, and Y. Zhao. Accelerating federated learning with cluster construction and hierarchical aggregation. *IEEE Transactions on Mobile Computing*, 22(7):3805–3822, 2022.
- [58] J. Wicaksana, Z. Yan, X. Yang, Y. Liu, L. Fan, and K.-T. Cheng. Customized federated learning for multi-source decentralized medical image classification. *IEEE Journal of Biomedical and Health Informatics*, 26(11):5596–5607, 2022.
- [59] Z. Yan, J. Wicaksana, Z. Wang, X. Yang, and K.-T. Cheng. Variation-aware federated learning with multi-source decentralized medical image data. *IEEE Journal of Biomedical and Health Informatics*, 25(7):2615–2628, 2021.
- [60] D. Yang, Z. Xu, W. Li, A. Myronenko, H. R. Roth, S. Harmon, S. Xu, B. Turkbey, E. Turkbey, X. Wang, W. Zhu, G. Carrafiello, F. Patella, M. Cariati, H. Obinata, H. Mori, K. Tamura, P. An, B. J. Wood, and D. Xu. Federated semi-supervised learning for covid region segmentation in chest ct using multi-national data from china, italy, japan. *Medical Image Analysis*, 70:101992, 2021.
- [61] M. Zhu, Z. Chen, and Y. Yuan. Feddm: Federated weakly supervised segmentation via annotation calibration and gradient de-conflicting. *IEEE Transactions on Medical Imaging*, 42(6):1632–1643, 2023.